Southeast-Asian J. of Sciences: Vol. 1, No 2(2012) pp. 195-209

ACCURACY IMPROVEMENT OF FINITE-DIFFERENCE TIME-DOMAIN METHOD FOR PHOTONIC CRYSTAL FIBERS

N. H. Vu[*] and I. K. Hwang[†]

[*] *Nguyen Tat Thanh University*
Ho Chi Minh City, Vietnam
e-mail: vnhai@ntt.edu.vn

[†] *Department of Physics,*
Chonnam National University, South Korea
e-mail: ikhwang@chonnam.ac.kr

Abstract

This paper describes computational errors found in Finite-Difference Time-Domain analyses of photonic crystal fibers, and proposes several techniques for the accuracy improvement. We first briefly introduce the FDTD computation scheme, and discuss about the optimization of various simulation parameters to obtain high accuracy with reasonable computation loads. The calculation of bending loss with good agreement with experimental data is demonstrated by proper selection of the computation domain. Finally, we propose the simulation based on a real fiber image to reflect irregularities and fabrication errors of fiber structures.

1. Introduction

First proposed in 1995 [1], photonic crystal fibers (PCFs) with silicaair microstructures attracted many researchers as these fibers have unique applications in ultrawide-band transmission, super continuum generation, high power delivery, novel optical amplifiers, and other functional devices. The typical

Key words: Optical fiber characterization, FDTD methods, optical fibers design and fabrication, optical fiber fabrication

PCF is made from a single material of undoped fused silica. Its cladding consists of a two dimensional photonic crystal with an air hole running along the length of the fiber [2]. One or more missing air holes at the center form the core of the PCF. Light waves can be guided in such a structure because the average index of the surrounding holey area is lower than the refraction index of the solid silica. The wide controllability of multiple parameters in the cladding structures lead to the emergence of various useful properties including endless single mode, flattened dispersion, and low bending losses. Theoretical studies of guided modes in PCFs have been performed based on a wide variety of techniques including the full vectorial effective index method [3], the plane wave expansion method [4], the finite element method [5], [6], the localized basis function method [7], and the finite-difference time domain (FDTD) method [8]. In this work, the FDTD technique [9] is considered for full analyses of microstructured or photonic crystal fibers.

Compared to other techniques, the FDTD method has the most simple and straightforward algorithm for solving time-dependent electromagnetic problems. The algorithm requires minimal assumptions and approximations, and thus provides fairly reliable results assuming that the spatial and temporal resolutions are sufficiently high. Currently, the FDTD technique is one of the most popular techniques for the study of 3-D photonic crystal structures such as nano-cavities and waveguides. Use of the FDTD method for analyses of PCFs has been proposed by M. Qiu [8], and calculation of elementary properties of PCFs was demonstrated [8]-[10].

Here we present the full aspects in computational errors of FDTD technique for analyses of PCFs. The paper is organized as follows. In Section 2, basic algorithm of the modified FDTD method used in this study is summarized. The simulation procedures and the interpretation of the results are described in detail. Section 3 explains the origin of errors in the FDTD method in connection with the computation loads, and discusses the optimization of simulation parameters for high accuracy with reasonable computation time. In Section 4, bending loss of a PCF is calculated using FDTD, and the discrepancy between the simulation and experimental results is highlighted. We identify the origin of the computation errors, and demonstrate that the errors are removed in the simulation with full cladding structures. In Section 5, we introduce a new function into the FDTD program which acquires an image file of a real fiber to reflect the irregularities of the fiber structure in the computation. It enables the investigation of the exact optical properties of a non-ideal fiber. Our conclusions are given in Section 7.

2. The periodic 3D-FDTD algorithm

The FDTD method is based on an algorithm that calculates the temporal evolution of the electromagnetic fields. Maxwells equations are solved at each discrete time by a so-called Yee-cell technique on a discrete three-dimensional mesh [8]. In Yees technique, the grids for the **E** and **H** fields are interleaved in the space as shown in Fig. 1. In a 3-D case, each **E** component is surrounded by four **H** components, and each **H** component is surrounded by four **E** components in computation. All the **E** components in the 3-D spaces are calculated first, and stored in memory for a particular time step using the **H** components previously stored in memory. Then, all the **H** components are updated and stored in memory using the **E** data just computed.

Therefore, the electric and magnetic field components are evaluated at different time steps and at different grid points, shifted by a half-period in both space and time. This process is repeated over multiple iterations.

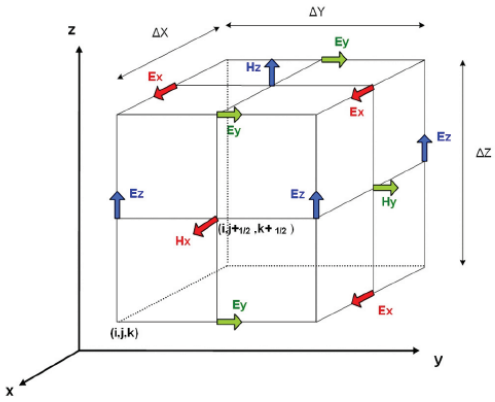

Fig. 1. Conventional Yee's 3-D mesh.

The optical pulse propagation along a fiber can be directly simulated if a computation structure includes a 3-D piece of fiber whose length is much longer than the pulse width. Such a simulation requires enormous memory and computation time, making the FDTD method impractical in such cases. However, when considering continuous wave propagation along the fiber, both the electromagnetic wave and dielectric structure remain constant along the fiber length, with the exception of a continuous increment of the optical phase. Therefore, the 3-D fiber structure can be reduced to an arbitrarily short length if a proper boundary condition is applied to account for the optical phase difference along the length, as shown in Fig. 2. Now the electromagnetic fields at the boundary layers can be updated using the fields at the opposite boundary layer after applying this phase difference.

For minimum calculation time and memory requirements, the computational domain may include just one computation grid along the z-axis with a size of Δz, which makes it a (effectively) 2-D structure. The propagation constant β along the z direction is specified by the user, and the phase difference between the upper and lower boundaries of a unit grid is $\Delta\varphi = \beta\Delta z$. Here we used both real and imaginary parts for $\mathbf{E}$ and $\mathbf{H}$ fields to define the optical phase. The absorptive layers are employed at the boundaries in the $x-y$ plane.

The optical variation (in phase or amplitude) along the z axis is usually much faster than those along the x and y axes, and thus a high grid resolution along the z axis is essential for accurate simulation. Here we adopted anisotropic resolution along each axis to increase the resolution for the z-axis, while keeping the resolution along the x- and y- axes low to reduce memory requirements and computation time.

This approach is very similar to the 2-D FDTD method reported previously [8]. The 2-D FDTD algorithm is definitely more compact than our 3-D case. However, it should be noted that our method retains the original 3-D FDTD algorithm, and thus it can handle both 3-D and 2-D structures without need of modification of the codes. (The boundary condition does nothing in the case of 3-D simulation since the absorptive layers are also imposed at the z-boundaries and the field intensities become zero.) Thus, it gives us greater flexibility compared to the 2-D FDTD method developed solely for 2-D waveguides or fibers [10].

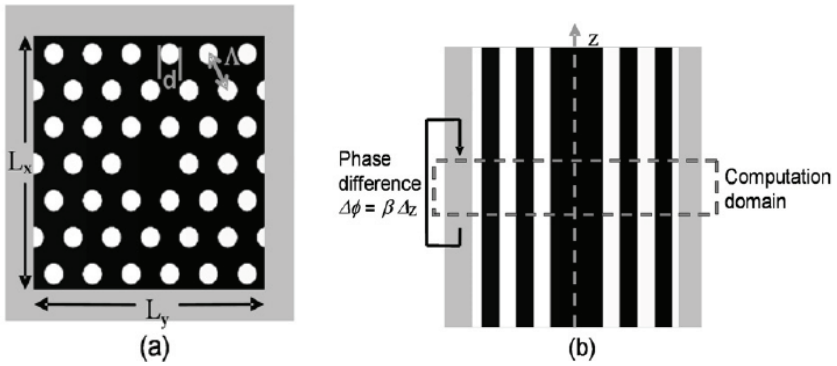

Figure 2: The cross section in xy plane and xz plane of the computational domain. Black represents silica regions and white represents vacuum. The gray region on the edges denotes the phase match layer (PML) [11].

The simulation results we obtain from the FDTD computation are only electromagnetic field distributions. To extract certain information from the raw data, an interpretation step is required. Usually more than one simulation run is required to obtain desired information. In this section, we describe our simulation procedure and discuss how we interpreted the simulation results.

The complete simulation procedure is as follows:

1. Setup: the computation structure (geometry and grid sizes $\Delta x, \Delta y, \Delta z$); field excitation (location, center frequency, frequency bandwidth, and field polarization); propagation constant (β); and field-observation points are described in the setup file.

2. Simulation: the **E** and **H** fields are computed and updated at each time step (T). Some of the field components are saved in storage for post-processing, as specified in the setup file.

3. Post-processing: The stored field data are analyzed in the time, frequency, and spatial domains.

To be able to observe the field profile of the fundamental mode, the optical source should selectively excite only the fundamental mode. It could be done in the second simulation by modifying the optical source so that it has the center frequency of $\omega_c = 3.601$ and very narrow bandwidth of $\Delta\omega = 0.051$, which corresponds to the pulse width of T = 5000. The propagation constant was kept the same as β_0. The frequency of $\omega = 3.601$ corresponds to the optical wavelength of $\lambda = 1550$ nm for the lattice constant of $\Lambda = 5.6\mu m$. The effective index of the mode was calculated to be $n_{eff} = \beta/\omega = 1.445$. This result provides a single data point in the dispersion curve, as shown in Fig. 3. The other data points were obtained by repeating the simulation with different values of β.

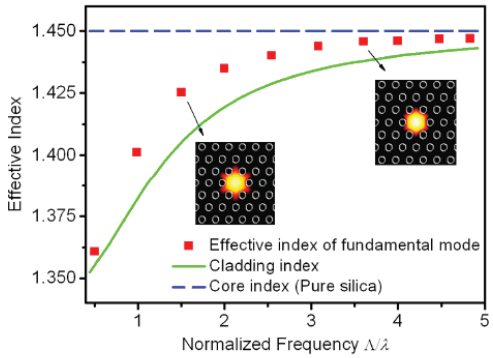

Fig. 3 Dispersion relation of PCF calculated using FDTD method.

3. Error analysis and optimization of FDTD parameters

A. FDTD parameters

The approximation used in the FDTD algorithm occurs when the time and spatial derivatives in Maxwells equations are replaced by the slopes between the neighboring data points with finite temporal or spatial differences. These finite sizes of time step and grid size result in the numerical errors in FDTD calculations. The finite length of the total computation time also affects the accuracy of the output in the frequency domain.

In this section, we investigate the influence of grid size (resolution), S-factor, and total computation time step (T_{max}) on accuracy and computation load, and suggest the optimal conditions under which reliable simulation can be performed with reasonable computing power.

The memory required for the storage of the **E** and **H** fields, and the total computation time, is determined by various parameters as shown in Table 1. Here, L_x and L_y are the structure sizes; $\Delta x, \Delta y$ and Δz are the grid sizes along the x, y and z directions; and $t_{max}(= T_{max}\Delta t)$ and Δt are the real time span and time step, respectively. S (S-factor) was introduced to determine the time step Δt. The size of the computational domain, L_x and L_y, should be big enough so that the mode intensity is nearly zero at the boundaries. Although typically $3 \sim 5$ layers of air holes are enough to obtain zero intensity at the boundaries, it should be reconsidered carefully in some cases as in section 4.

In the case of 2-D FDTD simulation for a PCF, the required memory size is usually well below 1 GB, and can be handled using a personal computer. However, the computation time ranges from minutes to days depending on the simulation conditions.

TABLE I
MEMORY SIZE AND COMPUTATION TIME REQUIRED FOR FDTD SIMULATION, DEPENDING ON VARIOUS PARAMETERS.

Memory size $\propto$	$\frac{L_x}{\Delta x}\cdot\frac{L_y}{\Delta y}$
Computation time $\propto$	$\frac{L_x}{\Delta x}\times\frac{L_y}{\Delta y}\times\frac{t_{\max}}{\Delta t}$ $\left(\Delta t=\frac{1}{cS}=\frac{1}{c\sqrt{\Delta x^{-2}+\Delta y^{-2}+\Delta z^{-2}}}\right)$
User setting parameters: L_x, L_y, L_z, Δx, Δy, Δz, S, $t_{\max}$	

B. Effects of grid sizes

The grid size should be small enough to describe the continuous variation of the **E** and **H** field distributions. In optical waveguides such as PCFs, the optical phase or amplitude changes much faster along the propagating direction (z-axis) compared to the transverse directions (x- and y-axes). $\Delta z < \lambda/20$ should be satisfied to describe the rapidly changing phase variation, while $\Delta x, \Delta y < \Lambda/10$ is adequate to describe the optical amplitude variation on the transverse plane.

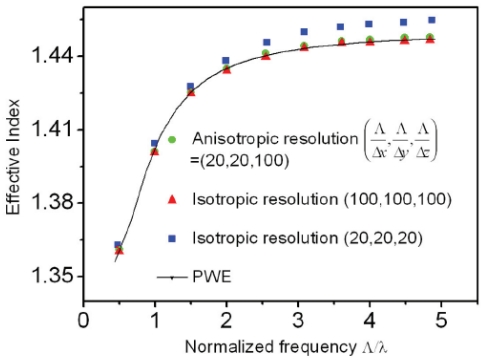

Fig. 4. Dispersion curves of PCF with different sets of resolutions compared to the results of the planewave expansion method (PWE).

To investigate this resolution-dependent accuracy of the FDTD simulation, we repeated the same simulation with different sets of resolutions. The FDTD results were compared with those from the planewave expansion method (PWE), which was performed with an exceptionally large number of planewaves to guarantee high accuracy. As shown in Fig. 4, the higher resolution of $\Delta x = \Delta y = \Delta z = \Lambda/100$ produced results closer to the PWE results. However, this simulation took computation time of 5x5x5 times longer than that of $\Delta x = \Delta y = \Delta z = \Lambda/20$.

On the other hand, when an anisotropic resolution of $\Delta x = \Delta y = \Lambda/20$ and $\Delta z = \Lambda/100$ was used, we achieved the same high accuracy with computation time increased by only $5 \sim 20$ times. This result demonstrates the usefulness of this approach. In the rest of the paper, the anisotropic resolution of $\Delta x = \Delta y = \Lambda/20$ and $\Delta z = \Lambda/100$ is used.

C. Two origins of error

The length of real time span t_max should be considered when calculating the optical frequencies of the modes excited with a given β. The mode frequencies are obtained by locating peaks of Ex(t) in the FFT data as explained in Section

2, and the accuracy of the peak location is related to the density of the FFT data, which is determined by the time span of the row data $E(t)$.

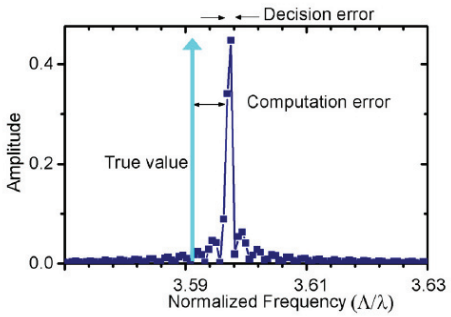

Fig. 5. Illustration of "computation error $\Delta\omega_c$" and "decision error $\Delta\omega_d$" in the mode frequency calculation process

Therefore, the total error in the mode frequency obtained by FDTD simulation came from two different origins as shown in Fig. 5. The first error, named computation error $\Delta\omega_c$ is due to the finite sizes of the grid and the time step. The second error is due to the finite length of the time span and is called decision error $\Delta\omega_d$. The total error can be written as

$$\Delta\omega = \sqrt{\Delta\omega_c^2 + \Delta\omega_d^2} \tag{1}$$

where $\Delta\omega_d = \frac{\Lambda}{\Delta z}\frac{S}{2t_{max}}$ and $\Delta\omega_c = f(\Delta x, \Delta y, \Delta z, S)$.

The decision error will be further reduced by using a curve fitting technique to find the peak position. The function for computation error $\Delta\omega_c$ is not found in an analytical form, and it can be determined only by numerical analysis. Attempts to reduce ω_c or ω_d are always accompanied by an increase in computation time as shown in Table 1. Therefore, it is important to create a balance between the two types of error to minimize the total error for a given computation time. For example, in Fig. 5, the computation error is much larger than the decision error. In this case, increasing spatial or time resolution should be more effective than taking a longer time span.

D. Effects of the S-factor

The time step Δt is defined by the parameter S as shown in Table 1. The condition for the S-factor is known as the Courant stability condition, which forces the propagation length of light taken during Δt to be shorter than one grid. When this condition is not satisfied, the amplitude of the EM field diverges as time goes on. Figure 6(a) shows an example in which the amplitude

of an electric field diverged after T = 4000 because the stability condition was not satisfied with S = 0.7. In this case, only the data for $T < 4000$ can be accepted for data analysis.

The S-factor affects the decision error $\Delta\omega_d$ in Eq. (1) as well as the stability of the FDTD calculation. To investigate S-factor dependence, we ran the same simulation with various values of S. Here, the computation time (or T_{max}) consumed for each simulation was kept equal. The results are shown in Fig. 6(b), with error bars indicating the magnitudes of the decision errors $\Delta\omega_d$.

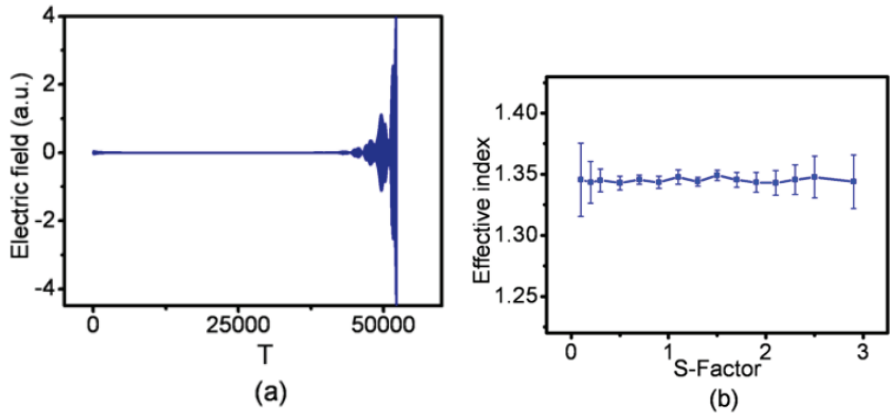

Fig. 6. (a). The divergence of electric field starting at T 40000 when S,=,0.7.
(b) The effective index of fundamental mode with decision errors depending on S-factor.

The error increases for small S-values since the field divergence occurred very early, and only a small portion of the data was available for the FFT. A large value of S also increased the error, as previously discussed. For $S > 1.2$, no divergence of the electric field was observed. Based on this study, the optimal value for the S-factor may be found in the range of $1.0 \sim 1.5$ for our applications.

4. Size effect of computational domain in bending loss calculation

A. Principle of bending loss calculation

The analysis of optical properties of bent fibers, including bending loss, are fundamental issues when considering reliable signal transmission [12]-[14] or optical sensing [15]. Recently, we reported the simulation of light propagation in bent fibers using 2-D FDTD [16]. To convert the 3-D structure of a bent fiber into a 2-D structure, the conformal transformation of the index distribution was

used as:

$$n_{eq}^2(x,y) = n^2(x,y)(1+\frac{2x}{R_b}) \qquad (Eq.2)$$

where R_b is the radius of the bend and $n(x,y)$ is the refractive index profile of the straight fiber [17]. The bottom part of Fig. 7(a) shows the transformed refractive index profile of a PCF with a bend radius of 5.5 mm.

Fig. 7(b) shows the recorded optical intensity E^2 at the center of the fiber as a function of time. The optical intensity corresponds to $I(t) =< E^2(t) >$. Here, we obtained the loss factor per unit time α' from curve fitting with the function $I(t) = I_0 exp(-\alpha' t)$. The loss factor per unit length is calculated from $\alpha = \alpha'/v$, where v is velocity of light in the fiber.

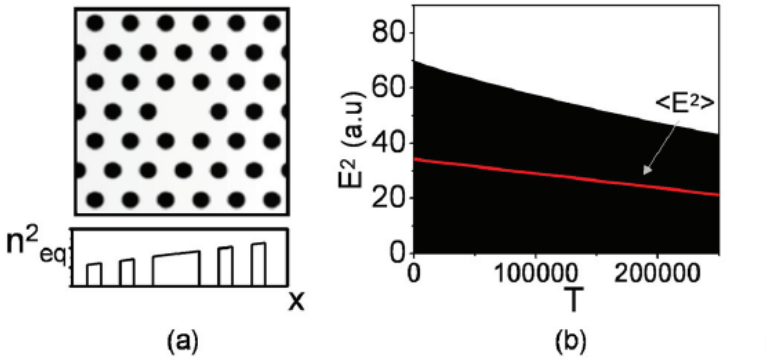

Fig. 7. Illustration of the simulation scheme: (a) a straight fiber with modified index profile, equivalent to a bent fiber; and (b) E^2 at the center of the fiber as a function of time, showing the attenuation of optical intensity due to bending loss.

B. Cladding boundary effect in bending loss

We calculated the bending losses of the LMA-8 PCF for several different bending radii, and the results are shown in Fig. 8 (a) together with the experimental data. In this calculation, two different sizes of computation structure were used: one with full cladding (the same as the real fiber used in the experiment), and the other with only a central part of the cladding. In most of the mode analyses, the latter has been enough for accurate simulation. However, in the bending loss analyses, the inclusion of full cladding was found to be essential to reproduce the details of the experimental data.

To understand the size effect of the computational domain, the dynamics of the optical field were observed in animations in Figs. 8 (b), (c), (d) and (e). In Fig. 8(b) and (c), one can observe a propagating field radiated from the center

toward the outside of the bend while the stationary core mode is blinking at its optical frequency. This energy propagation across the fiber is the cause of the bending loss. In Fig. 8 (d) and (e), the optical field in the holey cladding is not a purely propagating wave, but rather a mixture of propagating and stationary waves. This observation indicates the existence of optical back-reflection at the boundary of the holey-cladding which forms a weak cavity between the core and the boundary of holey cladding. The exceptionally large bending loss at the radius of ~ 4.5mm can be explained by a resonant coupling from the core to the cavity. Analyses of the cladding boundary effect on the bending loss are found in a previous report [18]. However, the FDTD simulation seems to be superior to other methods since it enables the direct observation of the optical field dynamics which provides better insight in investigation of the underlying mechanisms.

This demonstration emphasizes the importance of the computational domain size in specific simulations.

5. Simulation based on fiber images

It is often found that the structures of real PCFs have some irregularities or imperfections due to fabrication errors, and that their optical properties deviate from those expected based on simulations. Therefore the simulation for real fiber structures rather than ideal ones is important especially when the fiber contains large imperfections. One way to examine this effect is to intentionally impose certain irregularities on the simulation structure of the fiber, and investigate the level of fluctuation of optical properties as a function of the degree of irregularities. In [19], this approach was used to investigate the effect of PCF structural irregularities on birefringence. This kind of analysis is useful for the statistical prediction of general behavior. However, it is not applicable to the investigation of the exact optical properties of a given fiber with specific imperfections.

Here, we introduce a method which enables the analysis of fibers based on actual geometries. The new routine, added to our FDTD program, acquires an image file of a PCF and converts it to a matrix of dielectric constants to use as an input structure for the FDTD computation. Figure 9(a) shows a scanning electron microscope (SEM) image of a fiber to be converted to a matrix representing the simulation structure. Our program defines the silica/air boundaries based on the brightness of pixels, using a criterion set by a user. Figure 9(b) shows the computation structure and its simulation results. For comparison, the simulation was also performed for an ideal fiber structure for which the air holes were perfectly circular and arranged in a periodic lattice. In the ideal structure, the pitch and the hole size were defined by the average values of the real structures. It is clearly seen in Fig. 9(b) that the field intensity distribution

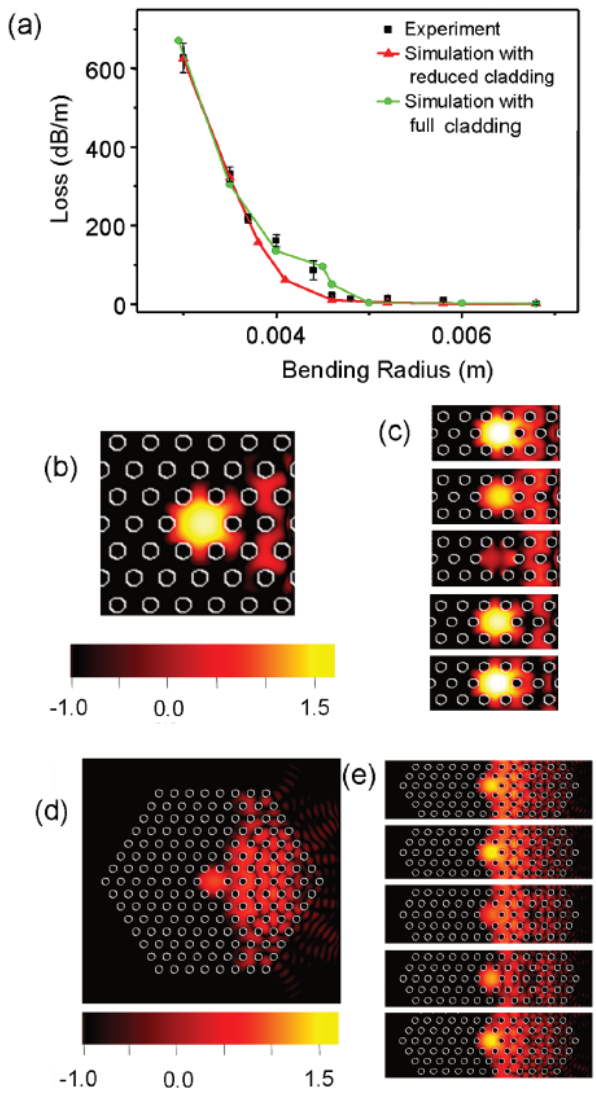

Fig. 8. (a) Bending loss as a function of bend radius and optical intensity distribution (in log scale) of a bent fiber with a radius of 5.5 mm from the simulations, with (b) reduced cladding, and (d) full cladding structure. (c) and (e) central regions of intensity profiles taken at successive times (Δt =1 fs) in one period of oscillation in case of reduced cladding and full cladding structure, respectively.

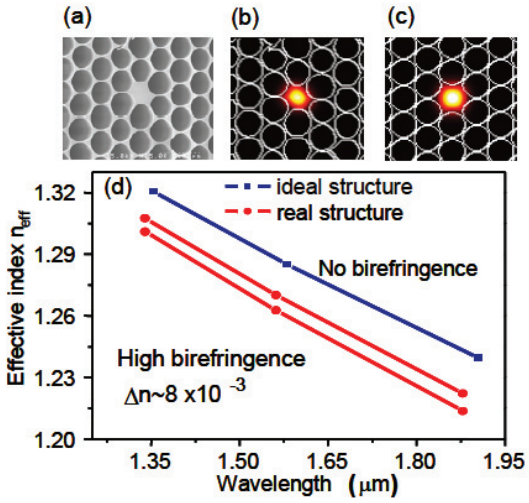

Fig. 10. (a). Real structure of PCF; (b) mode profile of real structure; (c) ideal structure; and (d) dependence of mode index on wavelength.

of the fundamental mode is asymmetric due to the elliptical core shape, whereas it is symmetric in the ideal structure shown in Fig. 9(c).

The most important characteristic induced by the asymmetry of the core geometry was unintentional birefringence. Figure 11(d) shows a part of the dispersion curve with splitting of the two polarization modes in the real PCF. The birefringence of $\Delta n \sim 8x10^{-3}$ observed here is higher than that of conventional polarization-maintaining fibers. The dispersion slopes of the two modes were also slightly different. The birefringence Δn calculated from the ideal structure was about 10^{-4}, which is below the numerical error of the FDTD method.

Using this technique, one can obtain the various optical properties discussed thus far for a given fiber. Our approach is expected be very useful in the analysis of experimental results associated with imperfect fibers.

6. Conclusions

We investigated FDTD techniques applicable to the analyses of photonic crystal fibers, showed that the accuracy of the computation can be enhanced by proper design of the simulation scheme. The simulation procedures and interpretation of the simulation results were described in detail. We investigated influence of various simulation parameters upon the accuracy of the simulation

results and computation loads, and the optimization of those parameters was discussed. We demonstrated the accurate calculation of bending loss with good agreement with experimental data by including the full cladding structures in the simulation. We also introduced a new function in the FDTD code, which acquires image file of a real fiber and converts it to a fiber geometry data for FDTD. This function enables us to investigate the optical property of a real fiber with imperfect geometries. Our study leads us to the conclusion that the FDTD method is an effective and powerful tool for investigation of microstructured or photonic crystal fibers as well as 3D micro cavities, if the simulation is properly planned. It enables us to directly peep into the electromagnetic waves flowing in micro systems, which provides us intuitive understating of optical properties. The high reliability of the simulation results come from its straightforward and rigid algorithm. The rapid advancement of the computer technology is also accelerating the wide applications of the FDTD method of which performances are highly dependent of the computing power.

Acknowledgment The authors give thanks to Dr. Se-Heon Kim and Prof. Yong-Hee Lee for their great help in development of FDTD program.

References

[1] T.A. Birks, J.C. Knight, P.St.J. Russell, Endlessly single-mode photonic crystal fiber Opt. Lett., vol. 22, pp. 961-963, 1997.

[2] P. Russell, Photonic crystal fibers Science, Vol. 299, pp. 358-362, 2003.

[3] X. Zhao, L. Hou, Z. Liu, W. Wang, G. Zhou, and Z. Hou, Improved fully vectorial effective index method in photonic crystal fiber, Appl. Opt., vol. 46, pp. 4052-4056, 2007.

[4] J. Arriaga, J. C. Knight, and P. St. J. Russell, Modeling the propagation of light in photonic crystal fibers Physica D, vol. 189, pp. 100106, 2004.

[5] F. Brechet, J. Marcou, , D. Pagnoux, P. Roy, Complete analysis of the characteristics of propagation into photonic crystal fibers by the finite element method Opt. Fiber. Technol., vol. 6, pp. 181191, 2000.

[6] H. Uranus and H. Hoekstra, "Modelling of microstructured waveguides using a finite-element-based vectorial mode solver with transparent boundary conditions" Opt. Express, vol. 12, pp. 2795-2809, 2004.

[7] D. Mogilevtsev, T. A. Birks, and P. St. J. Russell, Localized Function Method for Modeling Defect Modes in 2-D Photonic Crystals Journal of lightwave technology, vol. 17 , No. 11, pp. 2078-2081, 1999.

[8] M. Qiu, Analysis of guided modes in photonic crystal fibers using the finite-difference time-domain method Microwave Opt. Technol. Lett., vol. 30, pp. 327330, 2001.

[9] A.Taflove, S. C.Hagness, Computational electrodynamics: the Finite-Difference Time-Domain method , Artech House, 2005.

[10] Lou Shuqin, Wang Zhi, Ren Guobin, Jian Shuisheng, An efficient algorithm for modeling photonic crystal fibers Optical Fiber Technology, vol. 11, pp. 3445, 2005.

[11] J. P. Berenger, A perfectly matched layer for the absorption of electromagnetic waves J. Comput. Phys., vol. 114, pp. 185-200, 1994.

[12] M. Nielsen, J. Folkenberg, N. Mortensen, and A. Bjarklev, "Bandwidth comparison of photonic crystal fibers and conventional single-mode fibers" Opt. Express, vol. 12, pp.430-435, 2004.

[13] J. M. Fini, "Bend-resistant design of conventional and microstructure fibers with very large mode area", Opt. Express, vol. 14, pp. 69, 2006.

[14] H. Kuniharu, M. Shoichiro, G. Ning, W. Akira, Low bending loss single mode fiber to the home Journal of Lightwave Technology, issue 11, vol. 23, pp. 3494-3499, 2005.

[15] W. Belhadj, F. AbdelMalek, H. Bouchriha, Characterization and study of photonic crystal fibres with bends Materials Science and Engineering C , vol. 26, pp. 578 579, 2006.

[16] N. H. Vu, I. -K. Hwang, and Y. -H. Lee, "Bending loss analyses of photonic crystal fibers based on the finite-difference time-domain method," Opt. Lett., vol. 33, pp. 119-121, 2008.

[17] D. Marcuse, "Influence of curvature on the losses of doubly clad fibers," Appl. Opt., vol. 21, pp. 4208- 4213, 1982.

[18] Olszewski J., Szpulak M., Martynkien T., Urbanczyk W., Berghmans F., Nasilowski T., et. al, Analytical evaluation of bending loss oscillations in photonic crystal fibers Optics Communications, vol. 269:2, pp. 261-270, 2007

[19] I. -K. Hwang, Y. -J. Lee, and Y. -H. Lee, "Birefringence induced by irregular structure in photonic crystal fiber," Opt. Express, vol. 11, pp. 2799-2806, 2003